AMERICAN SOCIETY FOR MICROBIOLOGY | mSystems®

RESEARCH ARTICLE

Temporal Transcriptional Responses of a *Vibrio alginolyticus* Strain to *Podoviridae* Phage HH109 Revealed by RNA-Seq

Xixi Li,[a] Ce Zhang,[a] Xingkun Jin,[a] Fucheng Wei,[a] Fei Yu,[a] Douglas R. Call,[b] Zhe Zhao[a]

[a]Department of Marine Biology, College of Oceanography, Hohai University, Nanjing, China
[b]Paul G. Allen School for Global Animal Health, Washington State University, Pullman, Washington, USA

ABSTRACT Phage are thought to exhibit control over host genes during infection. As a preliminary investigation of the kinetics and magnitude of co-expression between phage and bacteria, we compared the global transcriptional profiles for *Vibrio alginolyticus* strain E110 and its lytic phage HH109 by using RNA sequencing. In total, 24.7% (1,143/4,620) of the host protein-coding genes were differentially expressed genes during infection (DEGs). Functional analysis of the host DEGs suggests that phage HH109 induced rapid and distinctive changes when compared with 60- and 120-min postinfection (mpi). Based on gene co-expression network analysis, an uncharacterized late gene *gp27* encoded by the phage HH109 was predicted to modulate the host's membrane transport and/or transcriptional regulation. Furthermore, expression of several bacterial virulence genes was downregulated while drug resistance genes were upregulated. This work contributes to an in-depth understanding of the reciprocal interactions of lytic phage HH109 and its pathogenic *Vibrio* host E110, and can provide new insights into the research and development of phage therapy against pathogenic *Vibrio* infections in the economically significant aquatic animals.

IMPORTANCE *Vibrio alginolyticus* is a common opportunistic pathogen that causes mass mortality in cultured marine animals. Phage HH109 lyses pathogenic *V. alginolyticus* strain E110 with high efficiency and thus serves as a useful model to understand the dynamic interplay of a phage and its host. Global transcriptomic responses of strain E110 post-HH109 infection were characterized by using RNA sequencing, elucidating step-by-step control by HH109, an antiphage-like responses, and the elevated expression of drug resistance. This study provides a detailed molecular description phage and *V. alginolyticus*, providing insight into better prevention and control of vibriosis in aquatic animals.

KEYWORDS bacterial lysis, lytic phage, RNA-seq, transcriptomic regulation, *Vibrio alginolyticus*

Vibrio alginolyticus, a Gram-negative opportunistic pathogen of marine aquatic organisms, is one of the causative agents of epidemic vibriosis that causes mass mortality of cultured fish, shellfish, shrimp, and coral reefs (1). And while uncommon, *V. alginolyticus* can cause otitis, wound, and intestinal infections in people (2). Treatment usually involves macrolide, tetracycline, or beta-lactam antibiotics for both medical and veterinary cases (3). Multidrug-resistant strains of *V. alginolyticus* have recently emerged across different marine ecosystems, including an offshore site, aquaculture environment, and water sediment (4, 5). We isolated *V. alginolyticus* strain E110 from the hepatopancreas of diseased white leg shrimp (*Penaeus vannamei*). E110 harbors virulence genes including a metalloprotease (*mtp*), alkaline serine protease (*asp*), type III secretion system (T3SS), and thermostable direct hemolysin (*tdh*).

Phage are viruses that can specifically recognize and infect a bacterial host and are found ubiquitously in many environments (6). More than a century ago, phage was

Editor Marta M. Gaglia, Tufts University

Address correspondence to Zhe Zhao, zhezhao@hhu.edu.cn.

The authors declare no conflict of interest.

Received 5 February 2022
Accepted 23 March 2022
Published 11 April 2022

used to treat bacterial infections (7), but the invention, ease of use, and ultimate adoption of antibiotics overshadowed the therapeutic potential of bacterial phage in the most parts of the world (8). With the growing crisis of antibiotic resistance, there is a renewed interest in using phage as therapeutics (9). Phage can be very selective with respect to susceptible strains, which is unique from the less specific activity of traditional antibiotics (10). Nevertheless, phage therapy can be limited by relatively narrow host range even within species, and the ligand-specific recognition mechanism is susceptible to resistance from spontaneous mutations (11).

Like all viruses, phage rely on host cell molecular and biochemical systems for reproduction prior to lysis (12). Lytic phage undergo adsorption to a cell surface, injection across the cell membrane, genome replication, transcriptional translation, virion assembly, and release to complete the infection cycle (13). Phage have developed various strategies to facilitate the release of virion progeny from infected host bacterial cells. Among them, the holin-endolysin system serves as a model for most dsDNA lytic phage (14), where holin-like proteins induce the formation of holes in the cytoplasmic membrane at a precise time to release the endolysin that accumulates in the host cell cytoplasm, resulting in cell burst (15). In addition, phage can use bacterial secretion systems to release endolysin that causes cell membrane depolarization, which in turn facilitates the endolysin-mediated cell lysis (16). Bacteria have also evolved a wide range of defense mechanisms against phage infection, including restriction-modification (RM) systems, "clustered regularly interspersed palindromic repeats" (CRISPR) loci together with CRISPR-associated (Cas) genes, and the abortive infection (Abi) system (17, 18). The process of phage-host interaction is a complex and dynamic arms race that is diverse in co-evolved interactions (19). *Escherichia coli* phage (20) and *Pseudomonas aeruginosa* phage (21) have served as our primary models for understanding host-phage interactions, but this limited scope may obscure understanding that could lead to improved phage therapy.

Previously, we isolated and identified a novel phage that was designated as HH109. This phage is a member of the *Podoviridae* family and it exhibits efficient lytic activity against *V. alginolyticus* strain E110. HH109 shares 99% sequence similarity with another phage VP670 (GenBank: KY290756), that was originally isolated from a different strain of *V. alginolyticus* (22). They both harbor 49 open reading frames (ORFs) but functional analysis has been limited to the holin and endolysin proteins (23). In this study, time-series RNA sequencing (RNA-seq) was employed to investigate the global effect of phage HH109 on the *V. alginolyticus* transcriptome. A myriad of differentially expressed genes (DEGs) were identified after phage infection, and gene-gene interaction networks provide insight into how the host and pathogen have co-evolved over time.

RESULTS

Lysis profiles of phage HH109 against *V. alginolyticus*. Phage HH109 prevented most growth of *V. alginolyticus* culture even with a multiplicity of infection (MOI) of 1:1,000 (Fig. 1A). An MOI of 0.01 was selected for subsequent analyses. A titer assay indicated that approximately 80% of phage HH109 is adsorbed to bacterial cells within 10-min incubation (Fig. 1B). After adsorption, there was a latent period of approximately 30 min during which the phage titer in the supernatant remained unchanged. The lysis period then began before moving into a stable period where there were approximately 32.5 PFU per infected cell (Fig. 1C).

The turbidity (OD_{600}) of HH109-infected and uninfected cultures increased at almost equal rates, suggesting that phage HH109 did not affect the growth rate of the *V. alginolyticus* culture with the first 20 min of infection (Fig. 2A), consistent with 86.1% of cells staining as live for this time point (Fig. 2B and C). The OD_{600} of phage-treated cultures at 60 and 120 min showed limited increase in turbidity (Fig. 2A), but progressive loss of viable cells although the change was not great between 60 and 120 min (Fig. 2B and C). Based on these findings, we elected to generate transcriptional profiles for 20-, 60-, and 120-min postinfection.

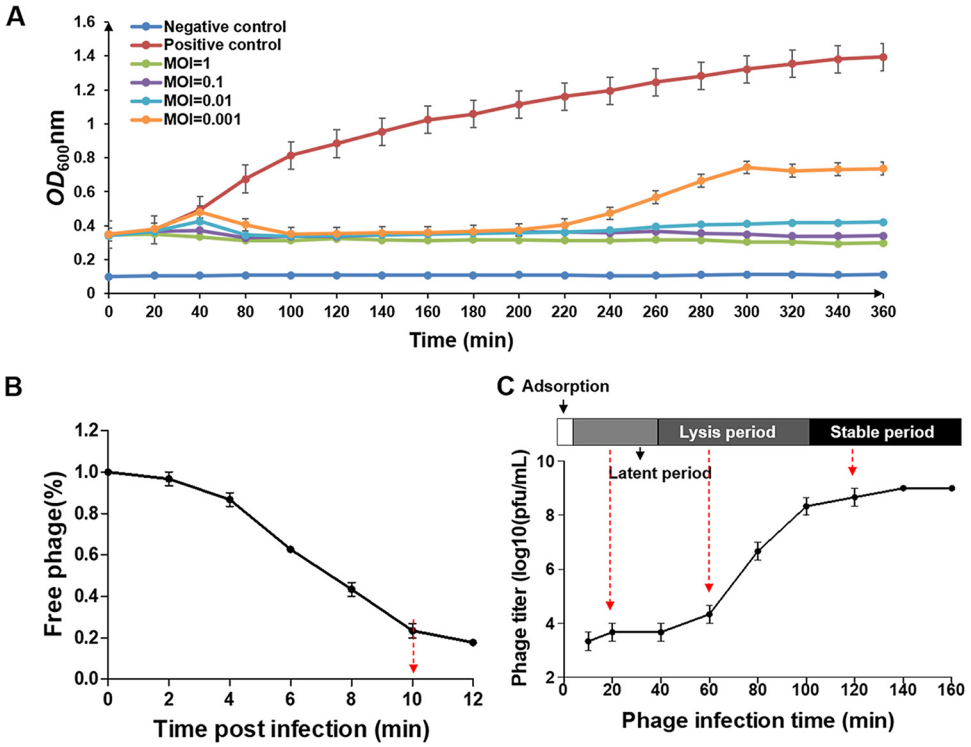

FIG 1 Infection dynamics of *V. alginolyticus* E110 by phage HH109. (A) Phage-mediated lysis of bacterial cultures at various MOI. Lysis was monitored by measuring the OD_{600}values for samples taken at the indicated times after infection. (B) Adsorption curve of HH109 to its host E110. The *x* axis shows the incubation time of HH109 and its host, and the *y* axis shows the percentage of the phage that did not adsorb to the host. (C) One-step growth curve of phage HH109. The *x* axis shows the incubation time of HH109 with its hosts after absorption for 10 min. The one-step growth curve of HH109 is from 10 to 160 mpi, which includes three periods: a latent period (divided into an eclipse phase and an intracellular accumulation phase), a lysis period, and a stable period. Red dotted arrows indicate the time points of sample collection. Data are displayed as the means ± SD from three independent experiments.

Temporal patterns of HH109 transcription. Transcriptional analysis revealed distinctive patterns of expressions of the 49 phage genes that included four groupings: (i) 14 ORFs peaked at 20 min (early); (ii) 17 ORFs at 60 min (middle); (iii) 15 ORFs peaked at 120 min (late); and (iv) three ORFs exhibited overall low-expression levels (*gp09*, *gp22*, and *gp13*) (Fig. 3). Some of the early genes, such as *gp46* and *gp45*, were annotated as important to host adsorption, which corresponds well with our findings. Most middle genes involved nucleotide metabolism-associated genes that are involved in phage genome replication and recombination/repair, including a DNA-directed DNA polymerase (*gp26*), a hydrolase/topoisomerase-primase (*gp23*), and a phosphomevalonate kinase (*gp37*). Late-expressed genes were mostly related to phage structural and lysis genes, like scaffolding protein (*gp44*), small terminase subunit (*gp04*), endolysin (*gp08*), and holin (*gp03*). The three hypothetical ORFs with a low relative expression were annotated as unknown proteins. Comparing the temporal transcriptional map of phage YerA41 and JD032, *gp08* and *gp03* with high similarity were expressed in the same phase, confirming our classification of HH109 genes (24, 25).

HH109 infection induces more host gene expression in the middle and late stages. The complete genome of strain E110 was sequenced for subsequent analysis of host-phage interactions using the Novaseq platform (GenBank: SRX10810502). The high-quality reads represented 99% of the raw reads, and high-quality sequence bases represented 99% of the raw data. The CheckM assessment and classification showed the genome assembly of E110 was 100% complete with 0.05% contaminated, ensuring a critical foundation for the inference of host-phage interactions (Table S2). It is worth mentioning that the genome contaminations reported by CheckM was due to presence

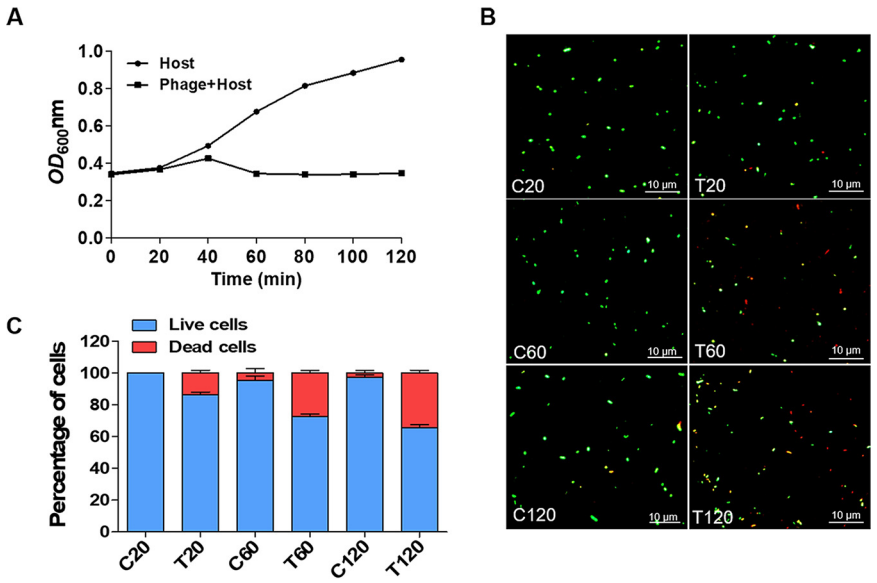

FIG 2 Viability of *V. alginolyticus* E110 for the transcriptional analysis. (A) Lysis was monitored by measuring the OD_{600} values for samples taken at the indicated times after infection. (B) Fluorescent staining: green means live bacteria, red means dead bacteria, yellow means live and dead bacteria. (C) Percentage of live and dead bacteria. Data are displayed as the means ± SD from three independent experiments.

of duplications of single-copy marker genes, which might represent the presence of paralogs in the E110 genome.

Using the same time points as previously and an MOI of 0.01, 24.7% (1143/4620) of recognized genes were differentially expressed (DEG) for treated versus untreated cultures (16.5% upregulated genes and 18.2% downregulated genes) (Fig. 4A). Among these DEGs, 743 and 824 genes were different at 60- and 120-min postinfection, respectively, while 37 genes were differentially expressed at 20-min postinfection (Fig. 4B). During early-stage infection, bacterial genes involved with nucleic acid biosynthesis were upregulated including ribonucleoside-diphosphate reductase subunit alpha (*nrdA*) and subunit beta (*nrdB*), single-stranded DNA-binding protein (*ssbB*), DNA helicase IV (*helD*), and putative transcriptional regulator (TetR/AcrR family) (*ycnC*). At the middle stage, endoribonuclease (*ybeY*), ribose ABC transporter ribose-binding lipoprotein (*rbsB*), oligopeptide transporter permease (*poT*), ribose ABC transporter permease (*rbsC*), a membrane transport protein (*rbsD*), TonB-dependent siderophore receptor (*tbrS*), ABC transporter ATP-binding protein (*rbsA*), and major facilitator transporter (*mfS*) genes were downregulated, and mainly involved in minor biosynthetic processes and transport. During the stable stage, DEGs included elongation factor G (*ef-G*), HAD family phosphatase (*serB*), malate dehydrogenase (*mdH*), fumarate hydratase (*FH*), glycogen synthase (*GS*), succinate dehydrogenase (*sdH)*, putative 3-hydroxyisobutyrate dehydrogenase (*hibadH*) which are mainly associated with metabolism, such as leucine metabolic process, cellular amide metabolic process, branched-chain amino acid metabolic process, citrate metabolic process, etc. That is, *V. alginolyticus* DEGs represented discrete function classifications for each of the three stages (Fig. 4C). The detailed expression data on DEGs are presented in Table S3.

To integrate complementary information from different databases and gain insight into the functions of DEGs, a Kyoto Encyclopedia of Genes and Genomes (KEGG) pathways analysis was also carried out. Based on the adjusted *P* value (*q*) and gene number (GN) of each KEGG pathway, 15 pathways were significantly changed ($q < 0.05$ and $GN > 3$) at one time point or more. From the time distribution of pathways, the DEGs mainly involved the host's nucleotide replication and metabolisms, such as DNA replication and pyrimidine metabolism in the early stage of infection. The most extensively changed KEGG pathways occurred in the middle and late stages of infection, which

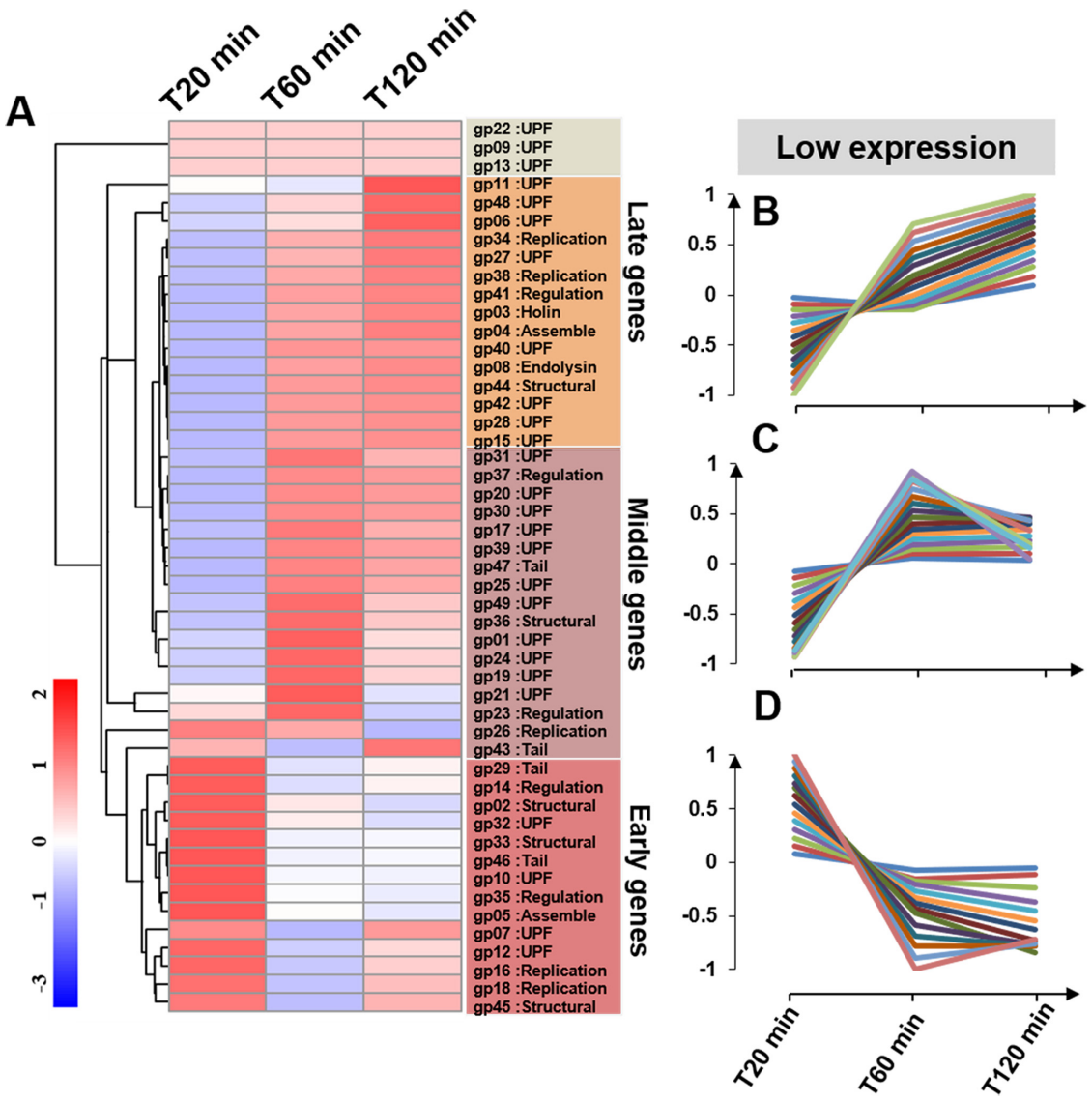

FIG 3 Temporal kinetic transcriptional profile of HH109 genome. (A) Hierarchical cluster heat map of HH109 genes. The normalized expression levels across all the time points are color-coded: red for high- and green for low-expression levels. Based on the read counts of genes, hierarchical cluster analysis was performed using ward.D2 and Minkowski methods (73). (B to D) A total of 49 ORFs of HH109 genes (*gp01* to *gp49*) were clustered into three clusters: early, middle, and late genes, also showing the time course of three transcript classes. The *y* axis showed the normalized expression levels of each gene. The positive sign represented a higher expression level, while the negative sign represented a lower expression level.

involved metabolites, such as carbohydrate metabolism, energy metabolic, lipid metabolic, *etc.* (Fig. 5). The detailed expression data on pathways are presented in Table S4.

Effects of HH109 infection on host *V. alginolyticus* drug resistance and virulence genes. We assessed the effects of phage HH109 infection on expression of 11 putative virulence genes and nine antibacterial resistance genes using both RNA-seq and qPCR. The results showed that most virulence-associated genes in *V. alginolyticus* were severely inhibited. In contrast, the antimicrobial resistance genes were mostly upregulated after the early stage (Fig. 6). The upregulation of these resistance-related genes or downregulation of these virulence-related genes indicated their potential participation in anti-phage infection in the host.

Phage-host interaction network. To assess potential interactions between phage and host gene expression, we constructed interaction networks (Fig. 7). Based on the sequential expression of the HH109 phage genes, classified into early, middle, late, and low-expression genes (Fig. 3A), we found a total of 2,275 co-expression relationships

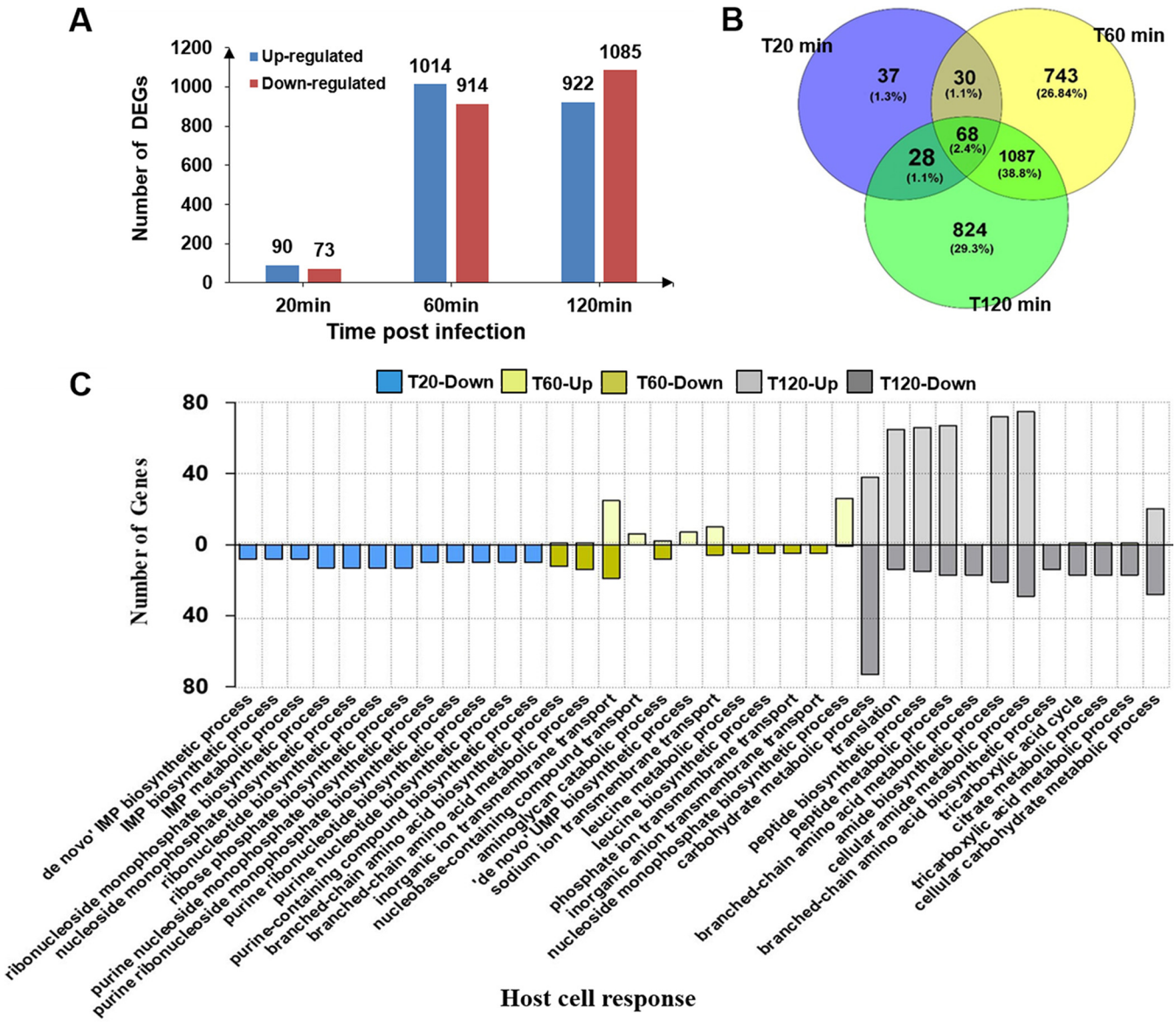

FIG 4 Analysis of differentially expressed genes (DEGs) of *V. alginolyticus* induced by phage infection. (A) The number and distribution of DEGs in different infection stages. (B) The Venn diagram shows the intersection of the number of DEGs at each time point. (C) GO analysis for the host cell response (the number of up- and downregulated genes). Upregulated genes are >0 and downregulated genes are <0.

($P < 0.01$, $|r| > 0.99$), including 436 negative correlations and 1,839 positive correlations ($P < 0.01$, $r > 0$) (Table S5). The correlation between HH109 and *V. alginolyticus* genes was quantified by a K-score range from one to five. Genes with higher K-scores (more links) were shown in bigger node sizes denoting their potential regulatory roles (Fig. 7). Large nodes included HH109 early genes *gp32* (uncharacterized protein), *gp35* (calcineurin-like phosphoesterase), middle genes *gp01* (viron protein), *gp36* (uncharacterized protein), *gp49* (uncharacterized protein), *gp37* (phosphomevalonate kinase), and late gene *gp42* (uncharacterized protein) (Fig. 7A). Sub-network linkages show genes with similar biological functions (26) such as the linkage between *gp16* (DNA-directed RNA polymerase, DdRp) and five host genes (transcriptional regulator, *gntR*, 23s rRNA, *lysR*, etc.) related to DNA replication and repair, nucleic acid metabolism (Fig. 7B). Genes *gp03* (Holin), *gp05* (large terminase subunit, TerL), *gp47* (tail protein), and *gp27* (hypothetical protein) composed one sub-network that could be defined as a transcription and membrane protein network (Fig. 7C). The inclusion of *gp27* suggests that it contributes to this function and further comparisons with the UniProt database indicated some amino acid

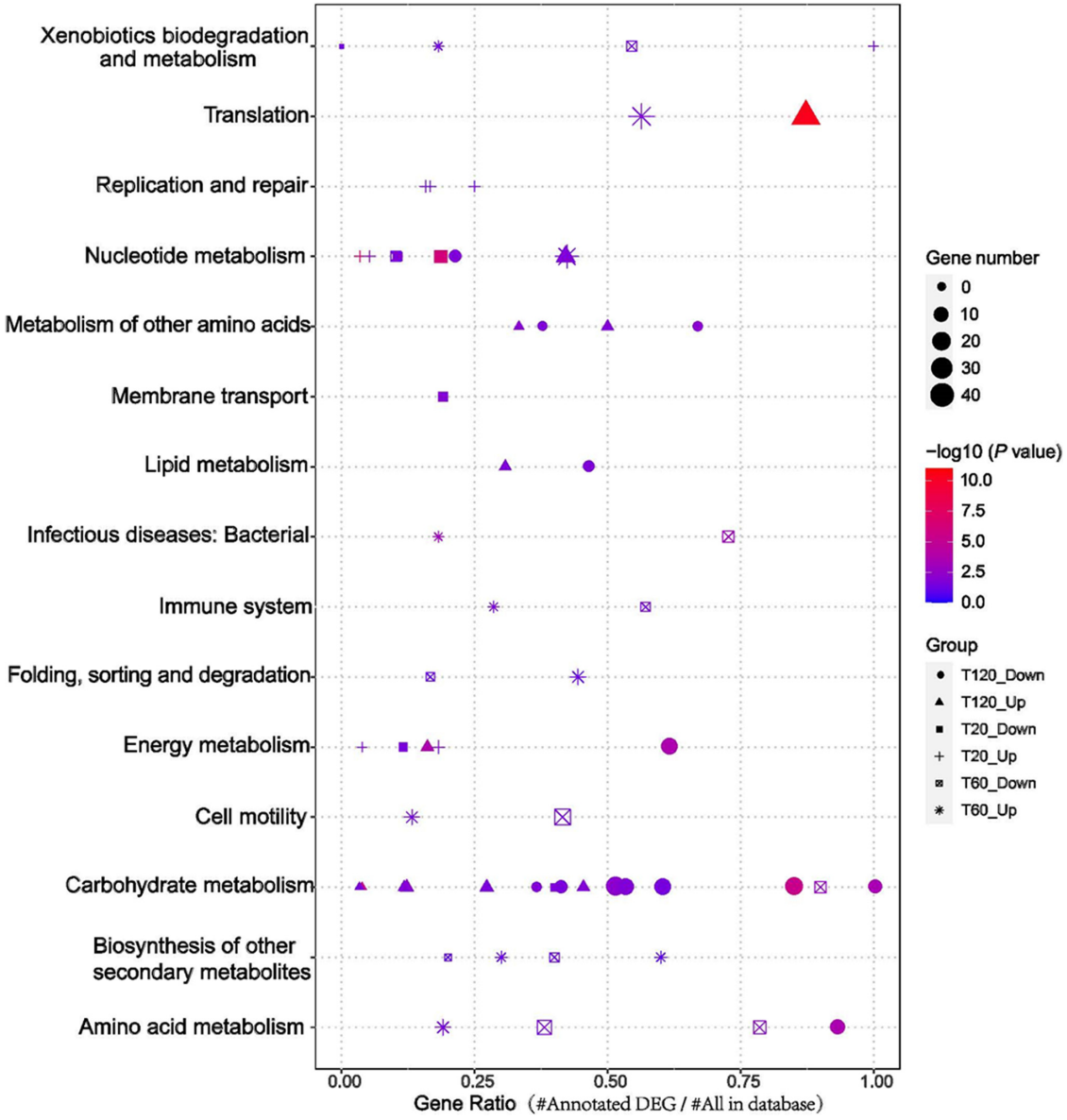

FIG 5 KEGG enrichment analysis of host DEGs (up- and downregulated genes) at each time point after HH109 infection. The shape of the point indicates the time points. The enrichment *P* value of each pathway was normalized as a negative log (*P* value) and is shown as a color gradient. The number of genes enriched in each pathway is represented by the size of the points. The ordinate is the KEGG pathway categories, the abscissa is the gene ratio and was calculated as number of DGEs annotated in a given KEGG pathway/total number of genes in a given KEGG pathway.

similarity to ORF68 (DNA-directed RNA polymerase I subunit RPA49; 53.3% similarity) and DNA helicase from *Pontibacillus marinus* (36.4% similarity).

Experimental validation of selected DEGs by qPCR. We used qRT-PCR to validate the results of RNA-seq for three phage genes (*gp01*, *gp35*, *gp37*) and seven bacterial genes (*hsdR*, *lysR*, *mfS*, *ef-tu*, *relE*) (Fig. 8). Comparative analysis showed that the expression pattern detected by qRT-PCR was a consistent directional change compared with RNA-seq, and change compared to RNA-seq with an overall correlation coefficient (*r*) of 0.87 ($n = 24$, $P < 0.0001$). These results are consistent with robust findings from the RNA-seq analysis.

DISCUSSION

The study of host-phage relationships is essential to understanding the mechanism of phage infection, coevolution of phages and hosts, as well as the complexity and

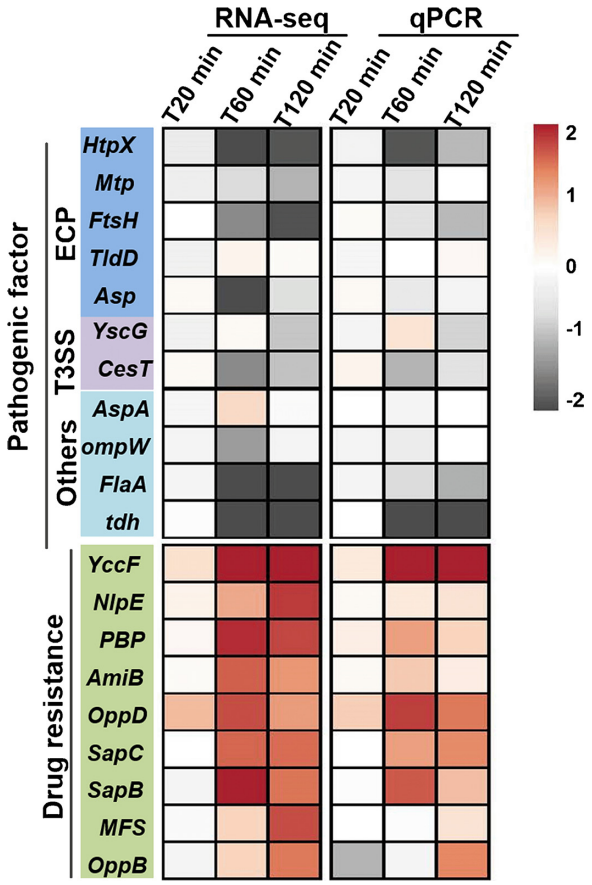

FIG 6 Expression of host genes related to pathogenicity and drug resistance after phage infection. Colors indicate upregulation and downregulation of the genes. ECP, extracellular products. T3SS, genes associated with type III secretion system of host.

diversity of phage-bacterium interactions (27). However, current knowledge about phage-host interactions is mainly based on a small number of bacterial hosts, including *E. coli*, *Acinetobacter baumannii*, *P. aeruginosa* (21, 28), and few studies consider both phage and host responses (28, 29). Therefore, probing the viral effects in a different but well-known bacterium, like *V. alginolyticus*, is essential for a deeper understanding of the interaction mechanism between host-phage. To this end, the temporal transcriptomic dynamic interactions between phage HH109 and its host *V. alginolyticus* were investigated using time-resolved RNA-seq. Our results demonstrated that the expression of HH109 genes follows the standard lytic phage pattern, including early, middle, and late stages. Transcriptional responses of *V. alginolyticus* to the phage HH109 infection were time-dependent, and presumably, many bacterial resources were needed for phage HH109 assembly and release in the middle and late infection stages. Moreover, the gene-gene interaction networks between HH109 and the host *V. alginolyticus* reflected probable protein-protein interactions between HH109 and host cells.

Previous work showed that lytic phages φSt2 and φGrn1 released progeny virions from *V. alginolyticus* after 20 min of infection, reaching the maximum at approximately 60 min when the infective cycle was completed (30). The latent period for the *V. alginolyticus* phage A318 was 20 min, followed by a 20-min rise period and an average burst size of approximately 72 phage particles per infected cell (31). In the present study, we found that the propagation cycle of phage HH109 was 100 min and the lysis period appeared at 40 to 100 min; moreover, progeny phage had not been released in the first 40 min (Fig. 1C). Compared with lytic phage VEN, these results suggested that the lytic cycle of HH109 is longer compared with other lytic *Vibrio* phages (32).

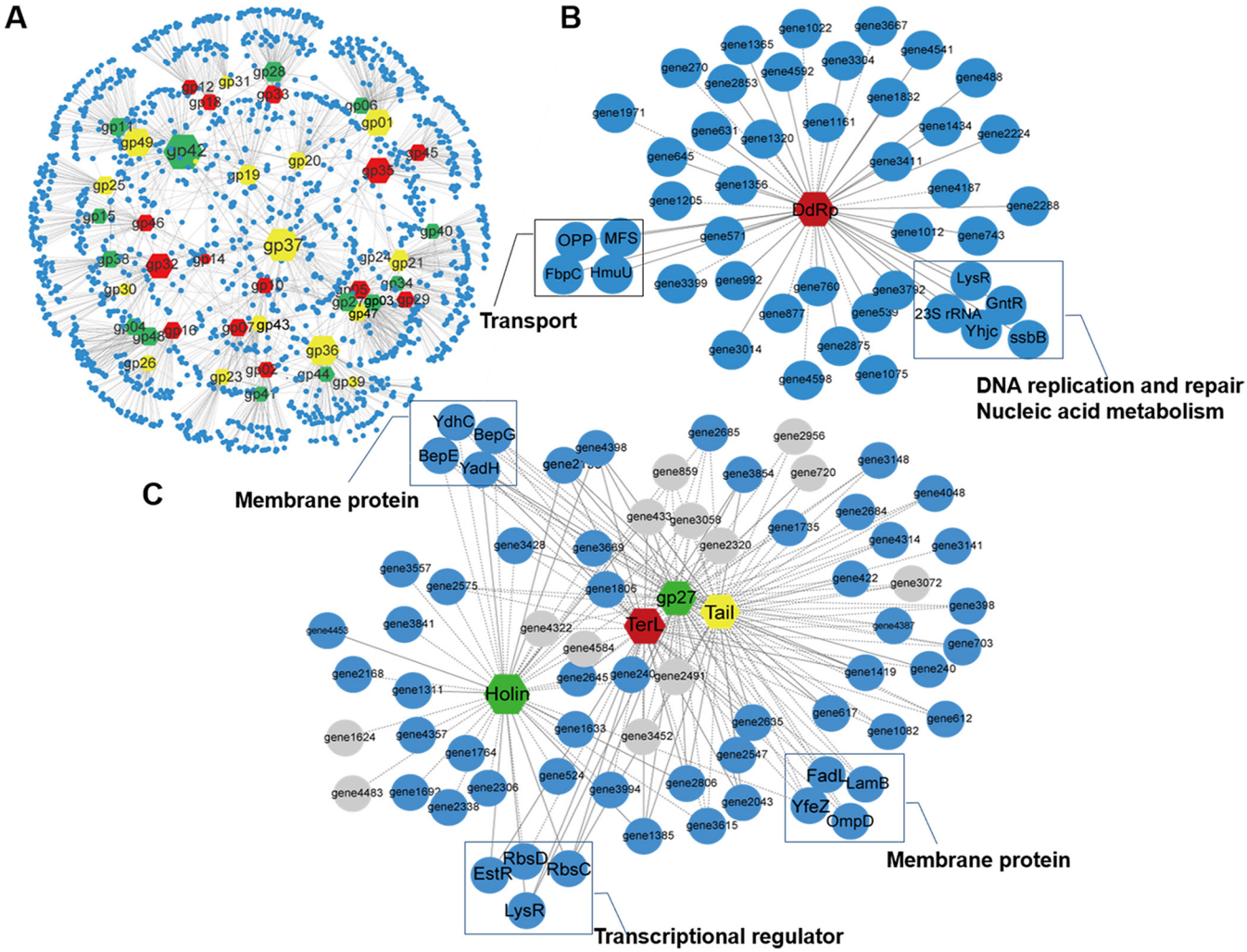

FIG 7 Gene co-expression network between HH109 and the host. (A) Main networks of host interactions centered on phage genes. (B) Positive and negative regulatory networks of early phage gene *DdRp*. (C) Positive and negative regulatory networks of phage gene *gp03* (Holin), *gp05* (TerL), *gp47* (tail protein), and *gp27* (hypothetical protein). The hexagons represent phage genes, three colors of nodes represent the early (red), middle (yellow), and late (green) HH109 genes, respectively; the blue and gray nodes are the annotated or hypothetical genes of host bacteria, respectively. The size of the nodes shows the interaction strength.

Adsorption is the first step in phage infection (33). Tail proteins serve as an adsorption organ for phage, and a series of subsequent infections are initiated when binding to receptors on the host cell surface (34). Like the tail protein, major capsid proteins adsorb to the pilus of *E. coli* and this initiates a cascade of processes involved in lysing *E. coli* (35). For the current study, tail protein (*gp46*) and major capsid protein (*gp45*) expression peaked during the early expression phase (Fig. 3). Endolysin and holin are involved with termination of the growth cycle and release viral progeny through host cell lysis (36), which is consistent with peak expression of these proteins during the late stage (Fig. 3).

The timing of the lytic cycle can vary between different phage. For instance, *Myoviridae* phage JD007 inhibited the growth of *Staphylococcus aureus* after coculture for 30 min at an MOI >1 (37). In contrast, *Podoviridae* phages VEN did not affect the growth rate of *V. alginolyticus* culture with MOI 10 within approximately an hour (32). For the current study, host cell genes involved with growth and division were not affected during the first 20 mpi (Fig. 4C and Fig. 5), consistent with different kinetics of lysis and phage-host genetic interactions. Others have shown that phage infection leads to specific protein-protein interactions whereby phage proteins inhibit, activate or otherwise redirect specific host proteins (38, 39) and this is presumably the case for phage HH109 as well with the

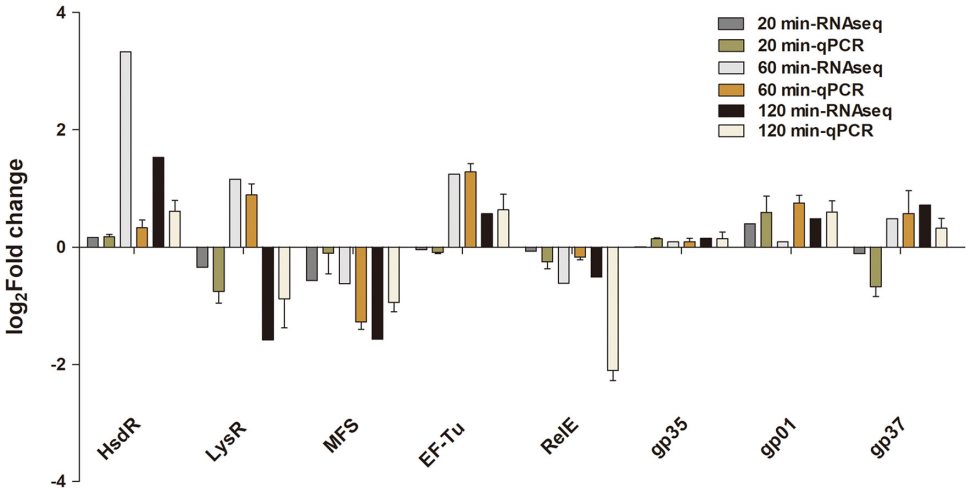

FIG 8 RT-qPCR validation of selected DEGs. Eight genes from *V. alginolyticus* and HH109 were compared by both qRT-PCR and RNA-seq. The qPCR results were normalized using *DnaK* and expressed as fold change (Log_{10} scale) by the comparative Ct method; moreover, the overall correlation coefficient for these pairwise comparisons were 0.87 ($n = 24$, $P < 0.0001$).

exception that we observed far more upregulated proteins compared with downregulated proteins, which is different from other studies (21, 28).

DEGs from the *V. alginolyticus* host could be broadly grouped as involving nucleic acid biosynthesis in the early infection phase, transport in middle phase, and metabolic processes in stable infection stages. For example, early phase upregulation included *nrdA* and *nrdB* host genes that encode ribonucleoside diphosphate reductase in phage T4, which is the key enzyme in the synthesis of DNA and catalyzes the first irreversible, committed step in the synthesis of dNTPs from rNDPs (40). YcnC is a putative transcriptional regulator of the TetR/AcrR family. These proteins are essential for the biosynthesis of deoxyribonucleotides from the corresponding ribonucleotides (41). Single-stranded DNA binding proteins (*ssbB*) are essential to the cell as they stabilize transiently open single-stranded DNA (*ssDNA*) intermediates, recruit appropriate DNA metabolism proteins, and coordinate fundamental processes such as replication, repair, and recombination (42). In addition, SsbB from *Bacillus subtilis* could contribute to some extent to stimulate replication of viral DNA (43). Furthermore, HelD is a helicase implicated in DNA repair and homologous recombination and interact with the RNA polymerase to stimulate effect on transcription cycling and elongation (44).

After 60 min of infection (middle phase), there is an induction of *YbeY*, which is involved in the processing of all three rRNAs and its products (RNase III, RNase R, and PNPase) that play important roles in both rRNA maturation and RNA degradation in *E. coli* (45), and thus *ybeY*, could have an impact in translation (46). Bacterial ABC transporters are involved in several diverse processes, including multidrug resistance, protein secretion, quorum sensing, and nutrient uptake (47). The members of SBP ABC transporters are located in the periplasm of Gram-negative bacteria and can accumulate solutes against large concentration gradients (48). In addition, genes *rbsA*, *rbsB*, *rbsC*, and *rbsD* constitute a ribose transport operon to provide a resource for carbon and energy synthesis (49). Therefore, the most extensively changed functions and pathways were seen at 60 min and involved the processes of transport and minor biosynthetic pathways in the present study.

Previous studies have not investigated changes in host gene expression during the stable phase following phage infection. For the present study, the majority of host cells were lysed by 120-min postinfection, leaving only small numbers of uninfected host (presumably phage HH109 resistant strains) or cellular debris (21). The host *V. alginolyticus* response to phage HH109 infection during the stable phase was markedly different. For example, there were more bacterial DEGs at the 120-min time point than those

during other periods (Fig. 4A). EF-G is a translation GTPase, which catalyzes tRNA movement during translation elongation, and promotes ribosomal recycling in the last step of translation. Moreover, EF-G is involved in various metabolic processes such as branched-chain amino acid metabolism (50). SerB proteins belong to the HAD phosphatase family, a relatively less-studied enzyme family that is involved in various metabolic processes including cellular-, phosphorus-, and phosphate-containing compound metabolism (51). SDH is a mitochondrial enzyme that participates in both the citric acid cycle and the electron transport chain. The SDH substrate succinate plays an important role in metabolic processes (52). Analysis of putative protein function indicated that DEGs of the host *V. alginolyticus* were significantly different from the other periods, mainly involving metabolism, especially carbohydrate metabolism in the present work (Fig. 4C and Fig. 5).

Like many other opportunistic pathogens, *V. alginolyticus* utilizes a variety of carbohydrates as sources of carbon and energy, and carbohydrates serve functions in combating host defenses and phage invasion (53). In addition, carbon sources, such as glucose, provide energy for the rapid growth of host bacteria and play a critical role in controlling cell death (54). Clustering of KEGG pathways revealed that carbohydrate metabolism was significantly inhibited during the infection period (Fig. 5), which may be important for keeping the host in a physiological state necessary for optimal phage development.

Previous reports have shown that prophages can promote the expression and induction of virulence/resistance traits when infecting *Enterococcus faecalis*, *P. aeruginosa*, *E. coli*, and *Bacillus anthracis* (55–58). For the current study, infection with the lytic phage HH109 was associated with downregulation of virulence-associated genes and upregulation of drug-resistance genes.

Gene co-expression network analysis has the potential to identify putative gene function (59). For example, using gene co-expression networks, Yang reported that a middle gene *gp34* of phage Abp1 had a negative interaction with numerous host ribosome protein genes (28), and the hypothetical proteins ORF68 and ORF59 of phage PaP3 might contribute to control of energy metabolism (21). In the present study, gene *gp27* of phage HH109 is included with Holin (*gp03*), large terminase subunit (*gp05*), and tail protein (*gp47*) that are involved in membrane transport and transcriptional regulation. Consequently, the uncharacterized gene *gp27* is likely to be involved these functions as well.

One potentially important weakness for this study involved the loss of approximately 25% of cells in the middle and stable phase samples due to lysis. It possible that this influenced the results through reduced assay sensitivity, or through genetic effects triggered by the presence of dead cells and lysate rather than due to direct effects of the phage.

In conclusion, global transcriptional analysis of phage HH109 and its host *V. alginolyticus* highlighted stage-dependent inhibition of host genes by HH109 and suggested that the late gene *gp27* of phage HH109 is involved in membrane transport and/or transcriptional regulation, and there is elevated gene expression associated with antibiotic resistance during lytic infection. Further, phage-mediated suppression of carbon resource associated genes from infected cells might indicate suppression of host defense mechanisms. Future functional studies (e.g., gene knockout, complementation, and heterologous expression) will provide more direct evidence of how phage and host genes and their products are involved during phage infection.

MATERIALS AND METHODS

Bacteria and phage isolation and preparation. *V. alginolyticus* strain E110 was originally isolated from shrimp in a South China aquaculture farm (23). Bacteria were cultured in LB liquid medium with 2% NaCl at 37°C. The phage HH109 was isolated using the *V. alginolyticus* strain E110 as host and purified using the standard double-layer agar method (30). The phage HH109 (3.8×10^{10} CFU/mL) was stored in Tris-SM buffer at 4°C.

Determination of the optimal multiplicity of infection (MOI). Aliquots of bacterial cells (2.4×10^{8} CFU/mL) were infected with phage HH109 at MOI of 0.001, 0.01, 0.1, or 1, respectively. Subsequently, the

cocultures were grown at 37°C with continuous shaking (180 rpm), and the optical density (OD) OD_{600} values were measured to evaluate the growth rate of bacterial cells using the Bioscreen C (Growth Curves Ab Ltd) at every 20-min interval over a 160-min time course.

Adsorption curve and one-step growth curve. The adsorption rate of phage HH109 on *V. alginolyticus* was determined in a previously described method (31). Briefly, bacterial cells were grown in 10 mL of LB broth with 2% NaCl to a density of 10^6 CFU/mL and then infected with the phage HH109 at MOI of 0.01 over a 10-min time course. The mixtures were collected at the indicated time point and pelleted at 14,000 $\times$ *g* for 30 s. Subsequently, the phage titer in the supernatant was measured by the double-layer agar plate method (31).

To ascertain the infection dynamics of phage HH109, the one-step growth curve of the phage was defined according to the method described previously (60). In brief, 20 mL of bacterial cells with a density of 10^6 CFU/mL were infected with phage HH109 at MOI of 0.01. After 10 min of adsorption, the mixtures were centrifuged at 14,000 $\times$ *g* for 1 min to remove the supernatant containing un-adsorbed phages. The pellets were washed twice with phosphate-buffered saline (PBS) and resuspended in 20 mL of fresh LB broth with 2% NaCl, then incubated at 37°C with shaking at 180 rpm. Samples (0.5 mL) were successively removed at indicated times over a 160-min period. Supernatants were obtained after centrifugation for 30 s at 14,000 $\times$ *g*, and the phage titer was immediately measured using the double-layer agar plaque method.

Whole-genome sequencing of *V. alginolyticus* strain E110. The genomic DNA of the *V. alginolyticus* strain E110 was extracted using a Puregene Yeast/Bact. kit B (Qiagen, Germany). The DNA samples' concentration, quality, and integrity were evaluated using Quant-iT PicoGreen dsDNA assay kit and 1% agarose gel electrophoresis, respectively. DNA Libraries were constructed with Illumina TruSeq DNA sample preparation reagents according to the manufacturer's instructions and sequenced using an Illumina NovaSeq instrument (Illumina, United States) owned by Shanghai Personal Biotechnology Co., Ltd. Adapter Removal was employed to remove linker sequences (61). The post-trimming high-quality reads were used to generate the genome assembly integrating A5-MiSeq v20150522 (62), SPAdes (63), pilon (64), respectively. The quality, completeness, and contamination of the *V. alginolyticus* genome were assessed using CheckM (65). The prokaryotic gene model was predicted by GeneMarkS (66) and annotated BLAST plus (67) using the NCBI-nr database.

Bacteria-phage interactions resolved by RNA-seq time-series. Based on the adsorption curve and one-step growth curve, 20 mL cultures of *V. alginolyticus* E110 were collected at 20, 60, and 120 min after phage HH109 infection at MOI of 0.01 and pelleted by centrifugation at 14,000 $\times$ *g* for 2 min. In parallel, uninfected E110 cells with equal volume and identical time points were collected as uninfected controls. All samples were immediately frozen at −80°C before RNA extraction. In addition, an aliquot of culture was taken at the three times to monitor the *V. alginolyticus* viability by optical density and fluorescence live/dead staining according to the manufacturer's instructions (Thermo Scientific, United States).

Total RNA was extracted from each sample using TRIzol reagent according to the manufacturer's instructions (Invitrogen Life Technologies). The concentration, quality, and integrity of the RNA samples were determined using NanoDrop ND-1000 UV spectroscopy (Thermo Scientific, United States) and 2100 Bioanalyzer (Agilent Technologies, United States) with RNA 6000 Nano kit (Walvax Biotechnology Co., Ltd.), respectively. The RNA samples with RNA integrity values (RIN) $\geq$ 8 were selected to construct cDNA libraries. Post-quality-control RNA samples were further subjected to mRNA enrichment by depleting rRNA with RiboZero magnetic kit (Bacteria; MRZMB126) supplied by Illumina. Random oligonucleotides and SuperScript III were used to synthesize the first strand cDNA. RNaseH was then used to degrade the RNA strand, and DNA polymerase I was used with dNTP and dUTP instead of dTTP to generate the second strand of cDNA. Remaining overhangs were converted into blunt ends via exonuclease/polymerase activity and the enzymes were removed by NEBNext Ultra Directional RNA Library Prep Kit for Illumina. After adenylation of the 3′ ends of the DNA fragments, Illumina PE adapter oligonucleotides were ligated to prepare for hybridization. cDNA library fragments were purified with the AMPure XP system (Beckman Coulter, Beverly, USA) to ensure preferential 400 to 500 bp length. The PCR cycles were adjusted to 15, and the final amplified libraries were quality checked using Bioanalyzer 2100 system (Agilent). Finally, quantitative PCR was used with the Kapa-SYBR FAST qPCR kit for Light Cycler 480 (KK4610) from Kapa Biosystems and a reference standard to construct equimolar pool of libraries. Each library was sequenced using TruSeq SBS kit v3-HS, in paired-end mode with the read length of 2 $\times$ 76 bp for the mRNA-seq experiments, using the HiSeq2000 instrument (Illumina) according to the manufacturer's protocol.

Bioinformatics analysis of RNA-seq data. FastQC was used to evaluate the quality of RNA sequencing reads. Raw data in the fastq format were preprocessed using sickle (version 1.2) (68). Clean data were obtained by removing adapter sequences, poly-N, and low-quality reads from raw data. All the downstream analyses were based on clean data with high-quality determined by Q30. Differential gene and transcript expression values were calculated according to the expected number of fragments per fragments per kilobase of exon model per million mapped fragments (FPKM). DESeq (v1.30.0) was used to detect differentially expressed mRNA, defined as transcripts with $|\log_2\text{FoldChange}|>1$ and *P*-value < 0.05. *P*-values were calculated by using a negative binomial distribution and corrected for compounding error by Benjamini-Hochberg (B & H). *V. alginolyticus* genes with a fold change value (FC) of $\geq$1.5 and a *q* value of $\leq$ 0.05 after phage HH109 infection were analyzed and classified. gene ontology (GO) analysis was performed with Blast2GO (BioBam) based on Wallenius' non-central hypergeometric distribution (http://bowtie-bio.sourceforge.net/index.shtml). KOBAS was used for the KEGG pathway analysis (69). Gene co-expression networks were developed by using Cytoscape 3.4.0 (70). Circos was used to draw the graph of the merged network for co-expressed genes (71).

RT-qPCR validation of RNA-seq results. To validate the RNA-seq data, 20 virulence- or drug resistance-related genes of host *V. alginolyticus*, five phage-bacteria interaction genes, and three HH109 genes were selected for qRT-PCR analysis. Primers were designed using Primer Premier 5 software (Table S1). RNA (1 μg) was reverse transcribed into cDNA using the PrimeScript RT reagent kit (TaKaRa, Japan) following the manufacturer's instructions with random primers. The PCR product was sequenced to ensure specificity of the amplified fragments. *DnaK* rRNA was used as an internal control to normalize the expression level, and all experiments were performed in triplicate. The qRT-PCR system was carried out in a 20-μL volume containing 0.4 μL one each of primer set (10 μM), 10 μL 2×SuperMix (Thermo Fisher Scientific), 8.2 μL ddH_2O, and 1 μL diluted cDNA template. The amplification protocol was set as follows: 94°C for 5 min, 40 cycles of 10 s at 94°C, 30 s at 60°C. Relative expression levels of target genes were calculated using the comparative Ct method with formula $2^{-\triangle\triangle Ct}$ (72).

Data availability. All the raw sequencing data generated from this study including DNA and RNA-seq are publicly available at the NCBI database under accession number PRJNA727447.

SUPPLEMENTAL MATERIAL

Supplemental material is available online only.

TABLE S1, DOCX file, 0.02 MB.

TABLE S2, XLSX file, 0.01 MB.

TABLE S3, DOCX file, 0.03 MB.

TABLE S4, DOCX file, 0.03 MB.

TABLE S5, XLSX file, 1.1 MB.

ACKNOWLEDGMENTS

This study was supported by the National Natural Science Foundation of China (31872597) Jiangsu Agricultural Science and Technology Independent Innovation Fund (CX [19]2033), and the Jiangsu Agriculture Research System (JATS[2021]519).

REFERENCES

1. Austin B. 2010. Vibrios as causal agents of zoonoses. Vet Microbiol 140:310–317. https://doi.org/10.1016/j.vetmic.2009.03.015.
2. Chen MX, Li HY, Li G, Zheng TL. 2011. Distribution of *Vibrio alginolyticus*-like species in Shenzhen coastal waters, China. Braz J Microbiol 42:884–896. https://doi.org/10.1590/S1517-83822011000300007.
3. Chen SC, Lee YT, Tsai SJ, Chan KS, Chao WN, Wang PH, Lin DB, Chen CC, Lee MC. 2012. Antibiotic therapy for necrotizing fasciitis caused by *Vibrio vulnificus*: retrospective analysis of an 8 year period. J Antimicrob Chemother 67:488–493. https://doi.org/10.1093/jac/dkr476.
4. Yasir M, Ullah R, Bibi F, Khan SB, Al-Sofyani AA, Stingl U, Azhar EI. 2020. Draft genome sequence of a multidrug-resistant emerging pathogenic isolate of *Vibrio alginolyticus* from the Red Sea. New Microbes New Infect 38:100804. https://doi.org/10.1016/j.nmni.2020.100804.
5. Marhual NP, Das BK, Samal SK. 2012. Characterization of *Vibrio alginolyticus* and *Vibrio parahaemolyticus* isolated from *Penaeus monodon*: Antimicrobial resistance, plasmid profiles and random amplification of polymorphic DNA analysis. Afr J Microbiol Res 6:4270–4276.
6. Zhan Y, Feng C. 2019. Bacteriophages that infect marine roseobacters: genomics and ecology. Environ Microbiol 21:1885–1895. https://doi.org/10.1111/1462-2920.14504.
7. D'Herelle F. 1917. Sur un microbe invisible antagoniste des bacilles dysentériques. C R Hebd Seances Acad Sci 165:373–375.
8. Kutter EM, Kuhl SJ, Abedon ST. 2015. Re-establishing a place for phage therapy in western medicine. Future Microbiol 10:685–688. https://doi.org/10.2217/fmb.15.28.
9. Gordillo Altamirano FL, Barr JJ. 2019. Phage therapy in the postantibiotic era. Clin Microbiol Rev 32:e00066-18. https://doi.org/10.1128/CMR.00066-18.
10. Tagliaferri TL, Jansen M, Horz HP. 2019. Fighting pathogenic bacteria on two fronts: phages and antibiotics as combined strategy. Front Cell Infect Microbiol 9:22–35. https://doi.org/10.3389/fcimb.2019.00022.
11. Pertics BZ, Szénásy D, Dunai D, Born Y, Fieseler L, Kovács T, Schneider G. 2020. Isolation of a novel lytic bacteriophage against a nosocomial methicillin-resistant *Staphylococcus aureus* belonging to ST45. Biomed Res Int 2020:5463801. https://doi.org/10.1155/2020/5463801.
12. Labrie SJ, Samson JE, Moineau S. 2010. Bacteriophage resistance mechanisms. Nat Rev Microbiol 8:317–327. https://doi.org/10.1038/nrmicro2315.
13. Berg JA, Merrill BD, Crockett JT, Esplin KP, Evans MR, Heaton KE, Hilton JA, Hyde JR, McBride MS, Schouten JT, Simister AR, Thurgood TL, Ward AT, Breakwell DP, Hope S, Grose JH. 2016. Characterization of five novel *Brevibacillus* bacteriophages and genomic comparison of *Brevibacillus* phages. PLoS One 11:e0156838. https://doi.org/10.1371/journal.pone.0156838.
14. São-José C, Parreira R, Santos MA. 2003. Triggering of host-cell lysis by double-stranded DNA bacteriophages: fundamental concepts, recent developments and emerging applications. Recent Res Dev Bacteriol 1:103–130.
15. Catalão MJ, Gil F, Moniz-Pereira J, São-José C, Pimentel M. 2013. Diversity in bacterial lysis systems: bacteriophages show the way. FEMS Microbiol Rev 37:554–571. https://doi.org/10.1111/1574-6976.12006.
16. Park T, Struck DK, Dankenbring CA, Young R. 2007. The pinholin of lambdoid phage 21: control of lysis by membrane depolarization. J Bacteriol 189:9135–9139. https://doi.org/10.1128/JB.00847-07.
17. Ishino Y, Shinagawa H, Makino K, Amemura M, Nakata A. 1987. Nucleotide sequence of the IAP gene, responsible for alkaline phosphatase isozyme conversion in *Escherichia coli*, and identification of the gene product. J Bacteriol 169:5429–5433. https://doi.org/10.1128/jb.169.12.5429-5433.1987.
18. Chopin MC, Chopin A, Bidnenko E. 2005. Phage abortive infection in lactococci: variations on a theme. Curr Opin Microbiol 8:473–479. https://doi.org/10.1016/j.mib.2005.06.006.
19. Stern A, Sorek R. 2011. The phage-host arms race: shaping the evolution of microbes. Bioessays 33:43–51. https://doi.org/10.1002/bies.201000071.
20. Elizabeth K, Daniel B, Georgia R, Erin B, Bob B, Burton G. 2018. From host to phage metabolism: hot tales of phage T4's takeover of *E. coli*. Viruses 10:387–394.
21. Zhao X, Chen C, Shen W, Huang G, Le S, Lu S, Li M, Zhao Y, Wang J, Rao X, Li G, Shen M, Guo K, Yang Y, Tan Y, Hu F. 2016. Global transcriptomic analysis of interactions between *Pseudomonas aeruginosa* and Bacteriophage PaP3. Sci Rep 6:19237–19249. https://doi.org/10.1038/srep19237.
22. Luo P, Yun L, Li Y, Tian Y, Liu Q, Huang W, Hu C. 2018. Complete genomic sequence of the Vibrio alginolyticus bacteriophage Vp670 and characterization of the lysis-related genes, cwlQ and holA. BMC Genomics 19:741. https://doi.org/10.1186/s12864-018-5131-x.
23. Li X, Zhang C, Wei F, Yu F, Zhao Z. 2021. Bactericidal activity of a holin-endolysin system derived from Vibrio alginolyticus phage HH109. Microb Pathog 159:105135. https://doi.org/10.1016/j.micpath.2021.105135.
24. Leskinen K, Pajunen MI, Vilanova MVG-R, Kiljunen S, Nelson A, Smith D, Skurnik M. 2020. YerA41, a *Yersinia ruckeri* bacteriophage: determination of a non-sequencable DNA bacteriophage genome via RNA-sequencing. Viruses 12:620–634. https://doi.org/10.3390/v12060620.

25. Li T, Zhang Y, Dong K, Kuo C-J, Li C, Zhu Y-Q, Qin J, Li Q-T, Chang Y-F, Guo X, Zhu Y. 2020. Isolation and characterization of the novel phage JD032 and global transcriptomic response during JD032 infection of *Clostridioides difficile* Ribotype 078. mSystems 5:e00017-20. https://doi.org/10.1128/mSystems.00017-20.
26. Weitz JS, Poisot T, Meyer JR, Flores CO, Valverde S, Sullivan MB, Hochberg ME. 2013. Phage-bacteria infection networks. Trends Microbiol 21:82–91. https://doi.org/10.1016/j.tim.2012.11.003.
27. Desiere F, Mcshan WM, Sinderen DV, Ferretti JJ, Brüssow H. 2001. Comparative genomics reveals close genetic relationships between phages from dairy bacteria and pathogenic *Streptococci*: evolutionary implications for prophage-host interactions. Virology 288:325–341. https://doi.org/10.1006/viro.2001.1085.
28. Yang Z, Yin S, Li G, Wang J, Huang G, Jiang B, You B, Gong Y, Zhang C, Luo X, Peng Y, Zhao X. 2019. Global transcriptomic analysis of the interactions between phage φAbp1 and extensively drug-resistant *Acinetobacter baumannii*. mSystems 4:e00068-19. https://doi.org/10.1128/mSystems.00068-19.
29. Wicke L, Ponath F, Coppens L, Gerovac M, Lavigne R, Vogel J. 2021. Introducing differential RNA-seq mapping to track the early infection phase for Pseudomonas phage ϕKZ. RNA Biol 18:1099–1110. https://doi.org/10.1080/15476286.2020.1827785.
30. Kalatzis PG, Bastías R, Kokkari C, Katharios P. 2016. Isolation and characterization of two lytic bacteriophages, ΦSt2 and ΦGrn1; phage therapy application for biological control of *Vibrio alginolyticus* in aquaculture live feeds. PLoS One 11:e0151101. https://doi.org/10.1371/journal.pone.0151101.
31. Lin YR, Chiu CW, Chang FY, Lin CS. 2012. Characterization of a new phage, termed ϕA318, which is specific for *Vibrio alginolyticus*. Arch Virol 157:917–926. https://doi.org/10.1007/s00705-012-1244-8.
32. Kokkari C, Sarropoulou E, Bastias R, Mandalakis M, Katharios P. 2018. Isolation and characterization of a novel bacteriophage infecting *Vibrio alginolyticus*. Arch Microbiol 200:707–718. https://doi.org/10.1007/s00203-018-1480-8.
33. Hu M, Zhang H, Gu D, Ma Y, Zhou X. 2020. Identification of a novel bacterial receptor that binds tail tubular proteins and mediates phage infection of *Vibrio parahaemolyticus*. Emerg Microbes Infect 9:855–867. https://doi.org/10.1080/22221751.2020.1754134.
34. Hyeon SH, Lim WK, Shin HJ. 2021. Novel surface plasmon resonance biosensor that uses full-length Det7 phage tail protein for rapid and selective detection of *Salmonella enterica* serovar Typhimurium. Biotechnol Appl Biochem 68:5–12. https://doi.org/10.1002/bab.1883.
35. Udom SU, Liu T, Enrique C, Huffman JB, Homa FL, Alex E. 2014. Major capsid reinforcement by a minor protein in herpesviruses and phage. Nucleic Acids Res 42:9096–9107. https://doi.org/10.1093/nar/gku634.
36. Nl A, Ys B, Qw A, Yi Q, Zhi CA, Ying WA, Sw B, Yuan SA. 2020. Cloning and characterization of endolysin and holin from *Streptomyces avermitilis* bacteriophage phiSASD1 as potential novel antibiotic candidates. Int J Biol Macromol 147:980–989.
37. Cui Z, Feng T, Gu F, Li Q, Dong K, Zhang Y, Zhu Y, Han L, Qin J, Guo X. 2017. Characterization and complete genome of the virulent *Myoviridae* phage JD007 active against a variety of *Staphylococcus aureus* isolates from different hospitals in Shanghai, China. Virol J 14:26–34. https://doi.org/10.1186/s12985-017-0701-0.
38. Roucourt B, Lavigne R. 2009. The role of interactions between phage and bacterial proteins within the infected cell: a diverse and puzzling interactome. Environ Microbiol 11:2789–2805. https://doi.org/10.1111/j.1462-2920.2009.02029.x.
39. Koerner JF, Snustad DP. 1979. Shutoff of host macromolecular synthesis after T-even bacteriophage infection. Microbiol Rev 43:199–223. https://doi.org/10.1128/mr.43.2.199-223.1979.
40. Cook KS, Wirak DO, Seasholtz AF, Greenberg GR. 1988. Effect of bacteriophage T4 DNA topoisomerase gene 39 on level of beta chain of ribonucleoside diphosphate reductase in a T4 nrdB mutant. J Biol Chem 263:6202–6208. https://doi.org/10.1016/S0021-9258(18)68772-1.
41. Härtig E, Hartmann A, Schätzle M, Albertini AM, Jahn D. 2006. The Bacillus subtilis nrdEF genes, encoding a class Ib ribonucleotide reductase, are essential for aerobic and anaerobic growth. Appl Environ Microbiol 72:5260–5265. https://doi.org/10.1128/AEM.00599-06.
42. Dickey TH, Altschuler SE, Wuttke DS. 2013. Single-stranded DNA-binding proteins: multiple domains for multiple functions. Structure 21:1074–1084. https://doi.org/10.1016/j.str.2013.05.013.
43. Mojardín L, Salas M. 2016. Global transcriptional analysis of virus-host interactions between phage ϕ29 and Bacillus subtilis. J Virol 90:9293–9304. https://doi.org/10.1128/JVI.01245-16.
44. Wiedermannová J, Sudzinová P, Kovaľ T, Rabatinová A, Šanderova H, Ramaniuk O, Rittich Š, Dohnálek J, Fu Z, Halada P, Lewis P, Krásny L. 2014. Characterization of HelD, an interacting partner of RNA polymerase from Bacillus subtilis. Nucleic Acids Res 42:5151–5163. https://doi.org/10.1093/nar/gku113.
45. Davies BW, Köhrer C, Jacob AI, Simmons LA, Zhu J, Aleman LM, Rajbhandary UL, Walker GC. 2010. Role of Escherichia coli YbeY, a highly conserved protein, in rRNA processing. Mol Microbiol 78:506–518. https://doi.org/10.1111/j.1365-2958.2010.07351.x.
46. Xia Y, Weng Y, Xu C, Wang D, Pan X, Tian Z, Xia B, Li H, Chen R, Liu C, Jin Y, Bai F, Cheng Z, Kuipers OP, Wu W. 2020. Endoribonuclease YbeY is essential for RNA processing and virulence in *Pseudomonas aeruginosa*. mBio 11:e00659-20. https://doi.org/10.1128/mBio.00659-20.
47. Basavanna S, Khandavilli S, Yuste J, Cohen JM, Hosie AH, Webb AJ, Thomas GH, Brown JS. 2009. Screening of Streptococcus pneumoniae ABC transporter mutants demonstrates that LivJHMGF, a branched-chain amino acid ABC transporter, is necessary for disease pathogenesis. Infect Immun 77:3412–3423. https://doi.org/10.1128/IAI.01543-08.
48. Higgins CF. 2001. ABC transporters: physiology, structure and mechanism–an overview. Res Microbiol 152:205–210. https://doi.org/10.1016/s0923-2508(01)01193-7.
49. Woodson K, Devine KM. 1994. Analysis of a ribose transport operon from *Bacillus subtilis*. Microbiology (Reading) 140:1829–1838. https://doi.org/10.1099/13500872-140-8-1829.
50. Klimova M, Senyushkina T, Samatova E, Peng BZ, Pearson M, Peske F, Rodnina MV. 2019. EF-G-induced ribosome sliding along the noncoding mRNA. Sci Adv 5:eaaw9049. https://doi.org/10.1126/sciadv.aaw9049.
51. Nakano I, Dougherty JD, Kim K, Klement I, Geschwind DH, Kornblum HI. 2007. Phosphoserine phosphatase is expressed in the neural stem cell niche and regulates neural stem and progenitor cell proliferation. Stem Cells 25:1975–1984. https://doi.org/10.1634/stemcells.2007-0046.
52. Dalla Pozza E, Dando I, Pacchiana R, Liboi E, Scupoli MT, Donadelli M, Palmieri M. 2020. Regulation of succinate dehydrogenase and role of succinate in cancer. Semin Cell Dev Biol 98:4–14. https://doi.org/10.1016/j.semcdb.2019.04.013.
53. Miwatani T, Shinoda S. 1971. Flagellar antigen of *Vibrio alginolyticus*. Biken J 29:389–394.
54. Doshi N, Mitragotri S. 2010. Macrophages recognize size and shape of their targets. PLoS One 5:e10051. https://doi.org/10.1371/journal.pone.0010051.
55. Rossmann FS, Racek T, Wobser D, Puchalka J, Rabener EM, Reiger M, Hendrickx APA, Diederich A-K, Jung K, Klein C, Huebner J. 2015. Phage-mediated dispersal of biofilm and distribution of bacterial virulence genes is induced by quorum sensing. PLoS Pathog 11:e1004653. https://doi.org/10.1371/journal.ppat.1004653.
56. Rice SA, Tan CH, Mikkelsen PJ, Kung V, Woo J, Tay M, Hauser A, Mcdougald D, Webb JS, Kjelleberg S. 2009. The biofilm life cycle and virulence of *Pseudomonas aeruginosa* are dependent on a filamentous prophage. ISME J 3:271–282. https://doi.org/10.1038/ismej.2008.109.
57. Veses-Garcia M, Liu X, Rigden DJ, Kenny JG, Mccarthy AJ, Alliso HE. 2015. Transcriptomic analysis of Shiga-toxigenic bacteriophage carriage reveals a profound regulatory effect on acid resistance in *Escherichia coli*. Appl Environ Microbiol 81:8118–8125. https://doi.org/10.1128/AEM.02034-15.
58. Raymond S, Fischetti VA, Aziz RK. 2009. The secret life of the anthrax agent *Bacillus anthracis*: bacteriophage-mediated ecological adaptations. PLoS One 4:e6532. https://doi.org/10.1371/journal.pone.0006532.
59. Wang S, Yin Y, Ma Q, Tang X, Hao D, Xu Y. 2012. Genome-scale identification of cell-wall related genes in Arabidopsis based on co-expression network analysis. BMC Plant Biol 15:1102–1114.
60. Li B, Zhang S, Long L, Huang S. 2016. Characterization and complete genome sequences of three N4-Like Roseobacter phages isolated from the South China Sea. Curr Microbiol 73:409–418. https://doi.org/10.1007/s00284-016-1071-3.
61. Schubert M, Lindgreen S, Orlando L. 2016. AdapterRemoval v2: rapid adapter trimming, identification, and read merging. BMC Res Notes 9:88–95. https://doi.org/10.1186/s13104-016-1900-2.
62. Coil D, Jospin G, Darling AE. 2015. A5-miseq: an updated pipeline to assemble microbial genomes from Illumina MiSeq data. Bioinformatics 31:587–589. https://doi.org/10.1093/bioinformatics/btu661.
63. Bankevich A, Nurk S, Antipov D, Gurevich AA, Dvorkin M, Kulikov AS, Lesin VM, Nikolenko SI, Pham S, Prjibelski AD, Pyshkin AV, Sirotkin AV, Vyahhi N, Tesler G, Alekseyev MA, Pevzner PA. 2012. SPAdes: a new genome assembly algorithm and its applications to single-cell sequencing. J Comput Biol 19:455–477. https://doi.org/10.1089/cmb.2012.0021.
64. Walker BJ, Abeel T, Shea T, Priest M, Abouelliel A, Sakthikumar S, Cuomo CA, Zeng Q, Wortman J, Young SK, Earl AM. 2014. Pilon: an integrated tool for

comprehensive microbial variant detection and genome assembly improvement. PLoS One 9:e112963. https://doi.org/10.1371/journal.pone.0112963.
65. Parks DH, Imelfort M, Skennerton CT, Hugenholtz P, Tyson GW. 2015. CheckM: assessing the quality of microbial genomes recovered from isolates, single cells, and metagenomes. Genome Res 25:1043–1055. https://doi.org/10.1101/gr.186072.114.
66. John B, Alexandre L, Mark B. 2001. GeneMarkS: a self-training method for prediction of gene starts in microbial genomes. Implications for finding sequence motifs in regulatory regions. Nucleic Acids Res 29:2607–2618.
67. Altschul SF, Gish W, Miller W, Myers EW, Lipman DJ. 1990. Basic local alignment search tool (BLAST). J Mol Biol 215:403–410. https://doi.org/10.1016/S0022-2836(05)80360-2.
68. Joshi NA, Fass JN. 2011. Sickle: a sliding-window, adaptive, quality-based trimming tool for FastQ files (version 1.33). https://github.com/najoshi/sickle.
69. Chen X, Mao X, Huang J, Yang D, Wu J, Dong S, Lei K, Ge G, Li CY, Wei L. 2011. KOBAS 2.0: a web server for annotation and identification of enriched pathways and diseases. Nucleic Acids Res 39:316–322.
70. Otasek D, Morris JH, Bouças J, Pico AR, Demchak B. 2019. Cytoscape automation: empowering workflow-based network analysis. Genome Biol 20:185–200. https://doi.org/10.1186/s13059-019-1758-4.
71. Krzywinski M, Schein J, Birol I, Connors J, Gascoyne R, Horsman D, Jones SJ, Marra MA. 2009. Circos: an information aesthetic for comparative genomics. Genome Res 19:1639–1645. https://doi.org/10.1101/gr.092759.109.
72. Kjl A, Tds B. 2001. Analysis of relative gene expression data using real-time quantitative PCR and the 2 $^{\Delta\Delta CT}$ Method. Methods 25:402–408.
73. Lee A, Willcox B. 2014. Minkowski generalizations of Ward's method in hierarchical clustering. J Classif 31:194–218. https://doi.org/10.1007/s00357-014-9157-8.